Kovove Mater. 64 2026 149–160
DOI: 10.31577/km.2026.3.149

Study on elemental segregation and mechanical properties improvement of Cu-Ni-Sn alloy via La alloying

Qin Xu[1], Sen Mao[1], Zhang Guoshun[2], Fu Yanling[2], Ruirun Chen[3]*

[1] *School of Mechanic and Electrical Engineering, Henan University of Technology, Zhengzhou 450001, P. R. China*
[2] *Henan Kefeng New Materials Co., Ltd., Zhengzhou 450001, P. R. China*
[3] *School of Materials Science and Engineering, Harbin Institute of Technology, Harbin 150001, P. R. China*

Received 15 March 2026, received in revised form 19 May 2026, accepted 17 June 2026

Abstract

To develop Cu-Ni-Sn alloys with high-performance in offshore oil and gas development, deep-sea exploration and other marine engineering equipment, a series of Cu-15Ni-8Sn-xLa alloys with varied trace additions of rare earth La (x = 0, 0.06, 0.12, 0.18, 0.24 wt.%) were synthesized in the present study, and influence of La addition on the phase constitution, microstructure transformation, element segregation, and mechanical properties of Cu-15Ni--8Sn alloy systematically examined. Results show that a new LaNiSn phase is formed in alloys with La content exceeding 0.12 wt.%, and the dimensional size of the new LaNiSn phase increases with increasing La content. The dendrite spacing of the alloys is first decreased and then increased by addition of La, dendrite spacing of alloy with addition of 0.12wt.%La is the smallest of 32.3 μm. Element segregation of different areas in the alloys first decrease then increase with increasing of La content, and the alloy with addition of 0.12wt.%La is the smallest for the grain refinement effect and transformation of ($\alpha + \gamma$) regions from lamellar to granular shape. Hardness, tensile strength, and ductility of the alloys show an initial increase trend followed by a decrease tendency with the gradual increase of La content, comprehensive mechanical properties of the alloy with addition of 0.12wt.%La are the best, and hardness, tensile strength, and ductility are 192.8 HV, 534.4 MPa, and 6.14 %, respectively. Therefore, addition of La can effectively reduce elemental segregation and improve mechanical properties of Cu-15Ni-8Sn alloys.

Key words: rare earth La, Cu-15Ni-8Sn alloy, microstructure, elemental segregation, mechanical properties

1. Introduction

Copper-based alloys are widely used to manufacture structural components for offshore oil and gas development, deep-sea exploration and other marine engineering equipment. Among them, copper-nickel--tin (Cu-Ni-Sn) alloys have become a research focus and are expected to be the next new generation of copper-based elastic materials due to their high strength, excellent thermal conductivity, and outstanding stress relaxation resistance. Cu-Ni-Sn alloys can be used in bad ocean environment required for strong corrosion resistance to seawater and excellent capacity to prevent from bio fouling attachment, and they have drawn substantial attention from researchers [1–4]. However, difference in surface tension of Cu (1303 MN m^{-1}), Ni (1758 MN m^{-1}), Sn (560 MN m^{-1}) and that in melting point of Cu (1083 ℃), Ni (1453 ℃), Sn (232 ℃) can lead to severe segregation during solidification process, and therefore reduce homogeneity of microstructure and decrease mechanical properties of the Cu-Ni-Sn alloys [5, 6].

Therefore, effective methods, such as micro alloying, were made to prevent element segregation and improve microstructure of alloys. Numerous studies demonstrate that introducing trace elements such as Fe, P, Nb, Ti, V, Al, and Si are capable of optimizing the mechanical properties of Cu-Ni-Sn alloys by refining grains and prevent element segregation [7–17]. Guo et al. [7] prepared Cu-15Ni-8Sn-xFe (x =

*Corresponding author: e-mail address: ruirunchen@hit.edu.cn

Table 1. Nominal and measured chemical compositions of alloy ingots (wt.%)

Sample	Nominal composition	Measured			
		Ni	Sn	La	Cu
TNXCNS-0La	Cu-15Ni-8Sn	14.82	7.93	–	Balance
TNXCNS-0.06La	Cu-15Ni-8Sn-0.06La	14.88	7.86	0.05	Balance
TNXCNS-0.12La	Cu-15Ni-8Sn-0.12La	14.94	7.81	0.11	Balance
TNXCNS-0.18La	Cu-15Ni-8Sn-0.18La	4.92	7.94	0.16	Balance
TNXCNS-0.24La	Cu-15Ni-8Sn-0.24La	15.10	8.04	0.21	Balance

0, 0.1, 0.3, 0.5 wt.%) alloys by vacuum induction furnace and found that tensile strength of alloy with 0.1wt.%Fe added was improved by 123 MPa compared with that without Fe added, and microhardness of the alloy reached 458 HV, which was improved by 30 HV compared with that without Fe added. Cheng et al. [9] prepared Cu-15Ni-8Sn-xNb alloys (x = 0, 0.8 wt.%) and found that grain size of alloy with 0.8wt.%Nb added decreased from 32 to 7 μm and tensile strength increased from 457 to 590 MPa compared with alloy without Nb added. Zhao et al. [11] found that addition of Ti can refine grain size of the alloys and prevent precipitation of discontinuous phases, therefore increase both tensile strength and elongation of Cu-15Ni-8Sn alloys. Li et al. [15] prepared $Cu_{80}Ni_{15}Sn_{5-x}Zn_x$ alloys and found that addition of element Zn can prevent segregation of Sn and achieve the improvement of mechanical properties for the alloys via solid solution strengthening effect. However, there are still exhibit certain limitations for these modification strategies. For instance, the addition of Fe into Cu-Ni-Sn alloys fails to improve the as-cast microstructure. Moreover, the addition of different Nb content has little effect on hardness of the alloy, which can be neglected in improving hardness of the alloys.

Rare earth elements have attracted extensive attention in modification of copper-based alloys due to their unique physical and chemical properties in recent years [18, 19]. Guo et al. [20] prepared Cu-2.35%Fe-0.03%P-0.1%Cr-xLa (x = 0, 0.1, 0.5, 0.8) alloys and found that addition of 0.8wt.%La can decrease grain size of the alloys from 150 to 40 μm and effectively improve mechanical properties of the alloys. Mao et al. [21] prepared Cu-30Ni-xRE (x = 0, 0.034, 0.095, 0.213) alloys by vacuum induction furnace and found that grain size of alloy with addition of 0.095 % RE was the smallest and the tensile strength was increased by 9.6 % to 308 MPa, however that of the alloy with 0.213 % RE added was decreased to 290 MPa. Chen et al. [22] found that rare earth La can refine grain of Cu-La alloys and improve elongation of the alloys by the purification effect of La, and addition of 0.32wt.%La into Cu-xLa alloy can improve tensile strength by 29 % from 188 MPa and microhardness from 61HV to 75HV, which may attributed to solid solution strengthening effect caused by La. According to the study by Li et al. [23], trace addition of La by 0.13 wt.% can decrease interdendritic spacing of Cu-0.45Cr-0.2Zr alloys and improve ultimate tensile strength as well as elongation of the ingots. Hu et al. [24] found that trace addition of La can significantly improve tensile strength and elongation of Cu-Ag alloys, however, excessive addition of La can lead to formation of coarse oxides and seriously damage the mechanical properties. Compared with other alloying elements, the trace amount of La can effectively reduce grain size, prohibit segregation, and improve mechanical properties of the alloys. Moreover, rare earth element La has a strong affinity with element Ni and element Sn, which can promote the formation of stable La-containing compounds.

Therefore, addition of the rare earth La can effectively improve the mechanical properties of copper-based alloys. However, there were still limited researches on mechanical properties improvement of Cu-Ni-Sn alloys via La alloying, and specific mechanism on improvement of mechanical properties for Cu-15Ni-8Sn alloys remain unclear. Accordingly, Cu-15Ni-8Sn-xLa (x = 0, 0.06, 0.12, 0.18, 0.24 wt.%) with varied trace addition of rare earth La were synthesized, and phases, microstructure, element segregation and mechanical properties were studied. The results of present study can provide theoretical and practical guideline for segregation control and property optimization of Cu-Ni-Sn alloys.

2. Experimental methods

A series of Cu-15Ni-8Sn-xLa (x = 0, 0.06, 0.12, 0.18, 0.24 wt.%) alloys added with varying contents of rare earth La were synthesized in the present study. The measured chemical compositions of different Cu-15Ni-8Sn-xLa alloys were determined by X-ray Fluorescence (XRF) Spectrometer in this study, the nominal and measured chemical compositions of the alloy ingots are shown in Table 1. Pure Cu, Ni, Sn, and La blocks with purity of 99.9% were selected as the starting materials, which were melted in a graphite crucible using a vacuum induction furnace. The raw

Table 2. Peak intensity of diffraction peaks for γ phase and LaNiSn phase

Alloy	Diffraction peak	Intensity
TNXCNS-0La	γ-(Ni,Cu)$_3$Sn	225
	LaNiSn	–
TNXCNS-0.06La	γ-(Ni,Cu)$_3$Sn	191
	LaNiSn	–
TNXCNS-0.12L	γ-(Ni,Cu)$_3$Sn	166
	LaNiSn	107
TNXCNS-0.18La	γ-(Ni,Cu)$_3$Sn	177
	LaNiSn	112
TNXCNS-0.24La	γ-(Ni,Cu)$_3$Sn	203
	LaNiSn	125

materials were melted with different power of 20, 40, and 60 kW for 3 min under protective atmosphere of argon. After the raw materials were fully melted, the power of the furnace was quickly increased to 65 kW and maintained for 5 min. The power supply was then cut off, and the melt was cooled in the crucible to room temperature. Five different cylindrical ingots with different La addition were achieved, of which the dimensional size are ø 40 mm × 240 mm. Cu-15Ni--8Sn-xLa alloys with different La contents are referred to TNXCNS-xLa, TNXCNS-0La, TNXCNS-0.06La, TNXCNS-0.12La, TNXCNS-0.18La, and TNXCNS--0.24La, respectively.

Samples with dimensions of 10 mm × 10 mm × 6 mm were cut from different ingots using HA400 wire electrical discharge machine to conduct phase analysis.

Phase analysis of various samples was conducted using an X-Ray Diffractometer (XRD, D8 ADVANCE) with Cu-Kα radiation source (20 kV, $\lambda = 0.154$ nm). Samples with dimensions of 10 mm × 10 mm × 6 mm were cut to conduct microstructure observation by a Field Emission Scanning Electron Microscope (FE-SEM, ZEISS Sigma 300) in backscattered electron (BSE) mode. Chemical composition of different phases for different samples was detected by energy dispersive spectroscopy (EDS) equipped on SEM.

"Dog-bone" shape tensile specimens with dimensional size of 30 mm × 8 mm × 2 mm were cut from the cylindrical ingots using an HA400 wire electrical discharge machine.WDW-50 type electronic universal testing machine was employed to carry out the tensile tests with a tensile rate of 5 mm min^{-1}. Each alloy's tensile strength and elongation were repeated 3 times, and the average was regarded as their final tensile strength and elongation. Microhardness of TNXCNS-xLa alloys with different La contents were measured using FM-ARS900 type automatic microhardness tester with load of 300 gf for 15 seconds. Microhardness of each alloy was measured at five points with the same distance on the sample, which was calculated by as average except the maximum and minimum of each sample.

3. Results and discussion

3.1. Phase analysis of TNXCNS-xLa alloys

Figure 1 shows X-ray diffraction (XRD) patterns of TNXCNS-xLa alloys with different contents of rare earth La, and Table 2 shows diffraction intensity of γ-(Ni,Cu)$_3$Sn phase and LaNiSn phase in TNXCNS--xLa alloys. Results show that TNXCNS-0La alloy without any addition of La and TNXCNS-0.06La alloy with 0.06wt.%La added are consisted of α-Cu phase and γ-(Ni,Cu)$_3$Sn phase, and LaNiSn phase is formed in TNXCNS-0.12La alloy with 0.12wt.%La added, TNXCNS-0.18La alloy with 0.18wt.%La added and TNXCNS-0.24La alloy with 0.24wt.%La added with more addition of La, shown in Fig. 1a. Diffraction intensity of γ-(Ni,Cu)$_3$Sn phase first decrease then increase with increasing addition of La into TNXCNS--0La alloy, and it is the lowest for TNXCNS-0.12La alloy with addition of 0.12wt.%La. Diffraction intensity of LaNiSn phase in TNXCNS-0.12La, TNXCNS--0.18La, and TNXCNS-0.24La alloys increases with more addition of La.

Furthermore, diffraction peak of (111) crystal plane for α-Cu phase shift to direction of lower 2θ

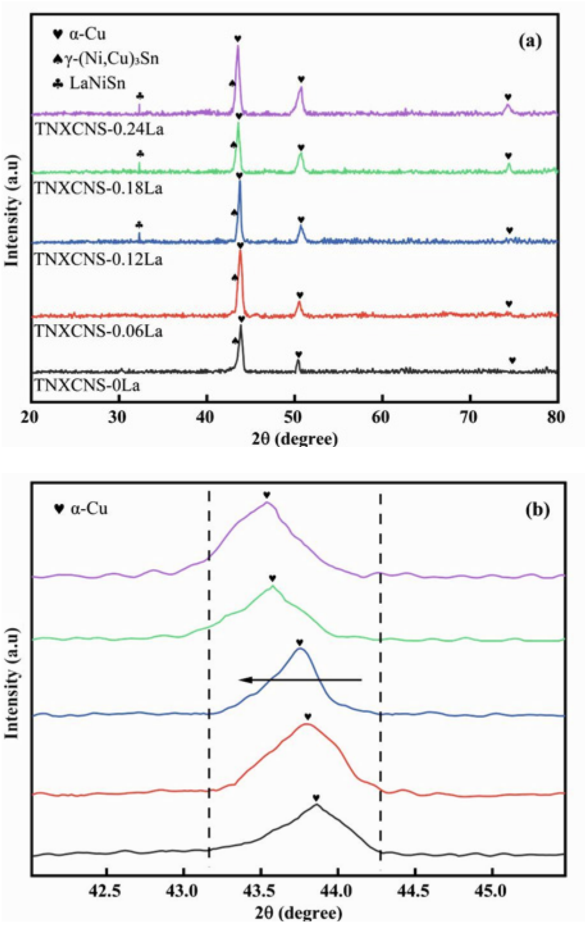

Fig. 1. X-ray diffraction analysis of TNXCNS-xLa: (a) XRD pattern and (b) diffraction peaks of (111) Cu.

with increasing addition of La into TNXCNS-0La alloy (shown in Fig. 1b), which may be attributed to lattice distortion caused by addition of La. The atomic radius of element Cu is 0.128 nm, while that of rare earth element La is 0.187 nm [25]. Therefore, atomic radius of Cu is smaller than that of rare earth La. According to Bragg's equation (Eq. (1)):

$$2d\sin\theta = \eta\lambda \tag{1}$$

interplanar spacing (d) decreases with increase of diffraction angle (θ) when wavelength of X-ray (λ) and diffraction order (η) remain constant. Therefore, addition of rare earth La into TNXCNS-0La alloy will lead to lattice distortion and subsequent lattice expansion of α-Cu phase, which can in turn leads to shift of the diffraction peak to direction of lower 2θ. The La atoms dissolved in α-Cu phase increases with further increase of rare earth La added in TNXCNS-0La alloy, and lattice expansion effect is even stronger, consequently, shift of diffraction peaks is more significant.

3.2. Microstructure analysis of TNXCNS-xLa alloys

Figure 2 shows microstructure of TNXCNS-xLa alloys with different contents of rare earth La and Table 3 shows EDS spectral of the alloys. Results show that TNXCNS-0La alloy without any addition of rare earth La is dendrite structure, and the average dendrite spacing is 51.1 µm. The alloy is mainly consisted of black α-Cu phase, white bone-like γ-(Ni,Cu)$_3$Sn phase and light grey transition ($\alpha+\gamma$) region around γ-(Ni,Cu)$_3$Sn phase, shown in Fig. 2a. The γ-(Ni,Cu)$_3$Sn phase precipitated in TNXCNS-0La alloy are mainly lath-shape and they are mainly distributed in the interdendritic area of the alloy. The local magnified image of the alloy illustrates that ($\alpha+\gamma$) lamellar tissue is eutectic with very small lamellar spacing.

TNXCNS-0.06La alloy with addition of 0.06wt.% La is also consisted of black α-Cu phase, white bone-like γ-(Ni,Cu)$_3$Sn phase and light grey ($\alpha+\gamma$) transition region, as is shown in Fig. 2b. Addition of 0.06wt.%La into TNXCNS-0La alloy lead to structure refinement of the alloy, and TNXCNS-0.06La alloy is dendrite structure with average dendrite spacing reduced to 42.8 µm. Some granular γ-(Ni,Cu)$_3$Sn phase formed in the alloy, dimensional size of γ-(Ni,Cu)$_3$Sn phase is smaller and the distribution gets more uniform. Rare earth La can be detected in γ-(Ni,Cu)$_3$Sn phase, which indicates that addition of La can also refine γ-(Ni,Cu)$_3$Sn phase, as shown in Table 3. The light grey transition ($\alpha+\gamma$) region in TNXCNS-0.06La alloy is smaller than that in TNXCNS-0La alloy, and the lamellar spacing get much smaller.

Formation of the LaNiSn phase can be further verified by thermodynamic calculations. The binary mixed enthalpy, mixed entropy and Gibbs free energy of the alloys were calculated based on the Miedema model [26, 27]. The mixed enthalpy of different element pair are, $\Delta H_{\text{La-Ni}} = -27\,\text{kJ mol}^{-1}$, $\Delta H_{\text{La-Sn}} = -53\,\text{kJ mol}^{-1}$, and $\Delta H_{\text{Ni-Sn}} = -4\,\text{kJ mol}^{-1}$, respectively. The negative mixed enthalpies indicates that the interatomic binding affinity is high from the perspectives of interatomic binding affinity and thermodynamic stability of phase precipitation, therefore, rare earth element La tends to bind with Ni and Sn. On the other aspect, the calculated Gibbs free energy (ΔG_{mix}) of the LaNiSn phase is $-130.44\,\text{kJ mol}^{-1}$. The above negative Gibbs free energy indicates that the formation of LaNiSn phase is thermodynamically favorable and the LaNiSn phase possesses the thermodynamic conditions to spontaneously precipitate in the alloys.

By further addition of La increased to 0.12 wt.%, new LaNiSn phase is formed in TNXCNS-0.12La alloy with addition of 0.12wt.%La, and the alloys is consisted of black α-Cu phase, white bone-like γ-(Ni,Cu)$_3$Sn phase, light grey transition ($\alpha+\gamma$)

region and LaNiSn phase, shown in Fig. 2c. TNXCNS-0.12La alloy is dendrite structure with average dendrite spacing further reduced to 32.3 µm. Most of γ-(Ni,Cu)$_3$Sn phase formed in the alloy are granular shape, dimensional size of γ-(Ni,Cu)$_3$Sn phase is further reduced. Some light grey transition ($\alpha + \gamma$) region of TNXCNS-0.12La alloy is change from lamellar shape to needlelike shape, and the lamellar spacing get even smaller.

Structure of TNXCNS-0.18La alloy with addition of 0.18wt.%La is quite similar to that of TNXCNS-0.12La alloy, the amount of LaNiSn phase is higher

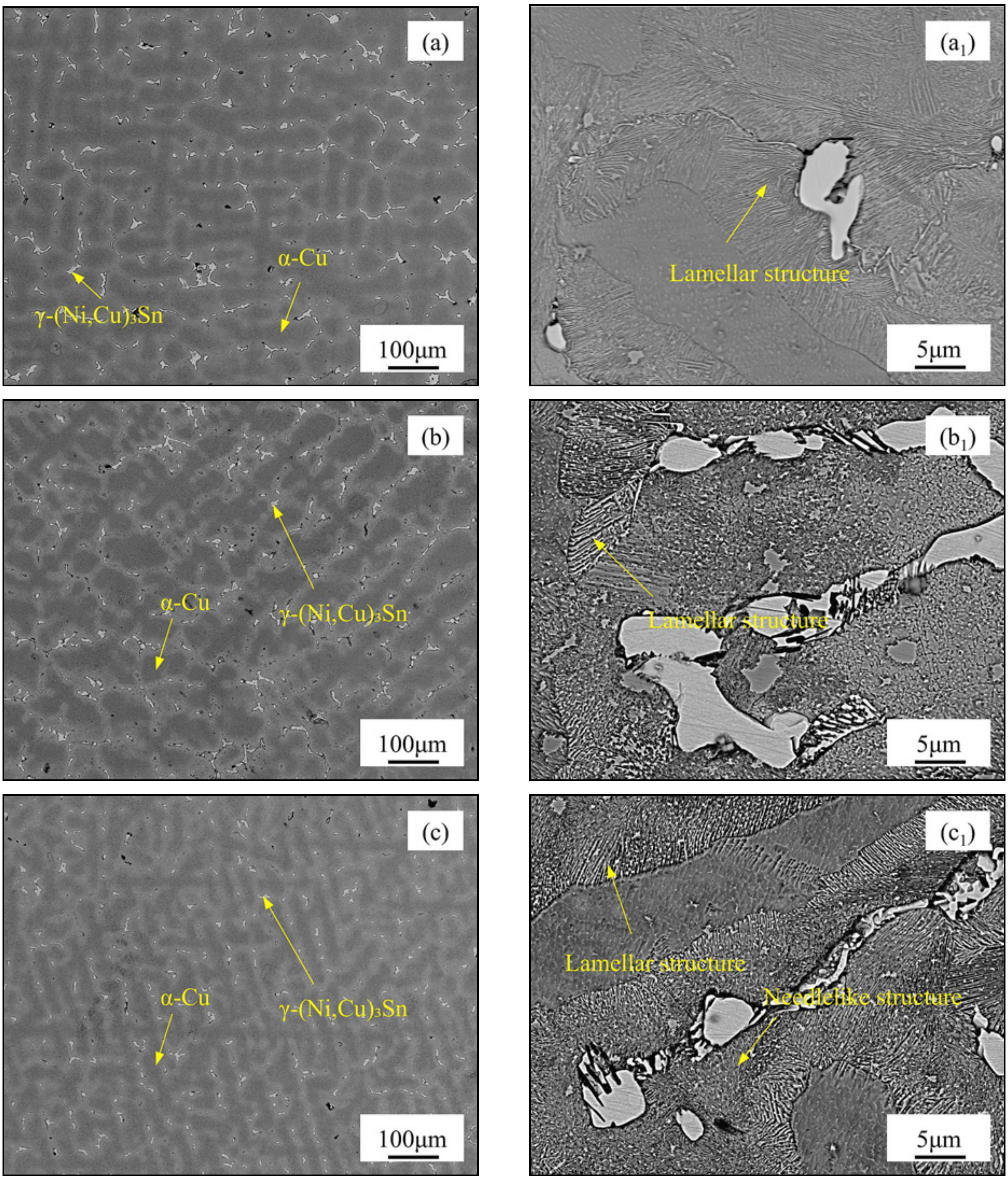

Fig. 2a–c. SEM images and average dendrite spacing diagrams of TNXCNS-xLa alloys: (a) TNXCNS-0La, (b) TNXCNS-0.06La, (c) TNXCNS-0.12La.

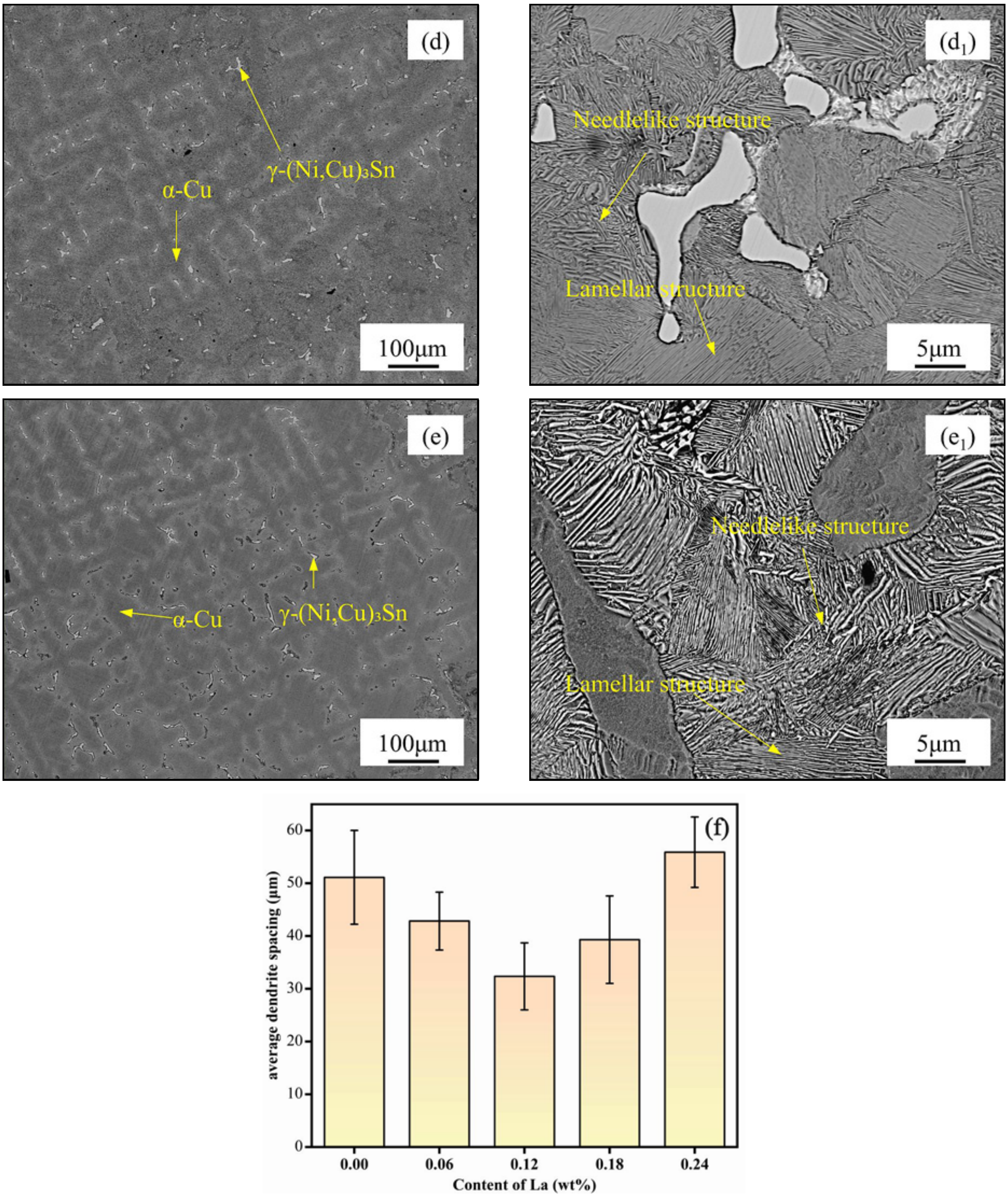

Fig. 2d–f. SEM images and average dendrite spacing diagrams of TNXCNS-xLa alloys: (d) TNXCNS-0.18La, (e) TNXCNS--0.24La, and (f) average dendrite spacing.

and the dimensional size is much bigger. TNXCNS--0.18La alloy is also consisted of black α-Cu phase, white bone-like γ-(Ni,Cu)$_3$Sn phase, light grey transition ($\alpha + \gamma$) region and LaNiSn phase, shown in Fig. 2d. TNXCNS-0.18La alloy is dendrite structure, and the average dendrite spacing begins to increase to 39.3 µm. γ-(Ni,Cu)$_3$Sn phase with granular shape formed in the alloy decreases and the lath-shape γ-(Ni,Cu)$_3$Sn phase formed in the alloy increases. Lamellar spacing of light grey transition ($\alpha + \gamma$) region with lamellar shape in TNXCNS-0.12La alloy increases, and ($\alpha + \gamma$) region with needlelike shape increases, too.

By further addition of La increased to 0.24 wt.%, no new phase forms in TNXCNS-0.24La alloy. TNXCNS-0.24La alloy with addition of La increased to

Table 3. Energy spectrum analysis of TNXCNS-xLa alloys with different La content (at.%)

Alloy	Possible phase	Cu	Ni	Sn	La
TNXCNS-0La	α-Cu	84.18	10.12	5.70	–
	$(\alpha+\gamma)$	62.67	17.28	20.05	–
	γ-(Ni,Cu)$_3$Sn	43.30	30.94	25.76	–
TNXCNS-0.06La	α-Cu	81.26	11.70	7.02	0.02
	$(\alpha+\gamma)$	66.31	16.53	17.11	0.05
	γ-(Ni,Cu)$_3$Sn	44.27	31.31	24.25	0.17
TNXCNS-0.12La	α-Cu	76.60	14.80	8.50	0.09
	$(\alpha+\gamma)$	66.61	18.27	15.01	0.11
	γ-(Ni,Cu)$_3$Sn	43.19	30.73	25.89	0.19
	LaNiSn	78.26	11.78	9.42	0.54
TNXCNS-0.18La	α-Cu	80.10	13.02	6.75	0.13
	$(\alpha+\gamma)$	69.11	18.28	12.37	0.14
	$\gamma-$(Ni,Cu)$_3$Sn	41.63	32.03	26.09	0.25
	LaNiSn	78.10	11.39	9.69	0.82
TNXCNS-0.24La	α-Cu	80.70	13.73	5.41	0.16
	$(\alpha+\gamma)$	71.46	18.43	9.91	0.2
	γ-(Ni,Cu)$_3$Sn	42.25	31.42	25.99	0.29
	LaNiSn	76.02	10.50	11.86	1.62

0.24 wt.% is also consisted of black α-Cu phase, white bone-like γ-(Ni,Cu)$_3$Sn phase, light grey pale grey transition $(\alpha+\gamma)$ region and LaNiSn phase, shown in Fig. 2e. However, the amount of LaNiSn phase is even higher and the dimensional size is much bigger. TNXCNS-0.24La alloy is dendrite structure with average dendrite spacing increased to 55.8 μm, which is even bigger than that of TNXCNS-0La alloy without any addition of La. Some huge and continuous γ-(Ni,Cu)$_3$Sn phase formed in the alloy.

Above all, certain addition of rare earth La higher than 0.12 wt.% to the TNXCNS-0La alloy can bring out the formation of the LaNiSn phase, and the dimensional size of the newly formed LaNiSn phase increases with the gradual increase of La content. Appropriate addition of rare earth La is capable of refining microstructure of the TNXCNS-0La alloy. Nevertheless, excessive La addition may make the microstructure of the alloy get coarser, and some may even be coarser than that of the La-free TNXCNS-0La alloy.

3.3. Elemental segregation of TNXCNS-xLa alloys

The essence of segregation is the phenomenon that different elements distribute unevenly in an alloy, and the degree of segregation is small when the difference in content of elements in different phase is small. Figure 3 shows EDS surface scan spectra of TNXCNS-xLa alloys. Results show that elemental segregation behavior are different for the five TNXCNS-xLa alloys with different addition of rare earth La. Specifically, element Ni in TNXCNS-0La alloy without rare earth La added is mainly rich in γ-(Ni,Cu)$_3$Sn phase, while element Sn is mainly distributed in γ-(Ni,Cu)$_3$Sn phase and $(\alpha+\gamma)$ eutectic area, shown in Fig. 3a. As is shown Table 3, the elements Ni and Sn in α-Cu is 10.12 and 5.70 %, respectively, and element Ni in $(\alpha+\gamma)$ eutectic area of the alloy is 17.28 at.%, while that of element Sn is 20.05 at.%. Element Ni in γ-(Ni,Cu)$_3$Sn phase is 30.94 at.%, while that of the element Sn is 25.76 at.%. Therefore, difference in content of elements Ni and Sn in different phases is significant, and elemental segregation of TNXCNS-0La alloy is consequently serious. In Chen's research [28], it was proposed that when the ratio of Ni to Sn in the Cu-Ni-Sn alloy was 2 : 1, the dendrite segregation was more pronounced.

When addition of La into TNXCNS-0La alloy is increased to 0.06 wt.%, element Ni in TNXCNS-0.06La alloy is also mainly rich in γ-(Ni,Cu)$_3$Sn phase, and element Sn is also mainly distributed in γ-(Ni,Cu)$_3$Sn phase and $(\alpha+\gamma)$ eutectic area, and element La is homogeneously distributed in the alloys, shown in Fig. 3b. However, element Ni and Sn in α-Cu is 11.70 and 7.02 %, respectively, and element Ni in $(\alpha+\gamma)$ eutectic area is decreased to 16.53 at.%, while that of element Sn is decreased to 17.11 at.%. And element Ni in γ-(Ni,Cu)$_3$Sn phase is 31.31 at.%, while that of element Sn is 24.25 at.%. Therefore, addition of La can reduce element segregation of Ni and Sn in the alloy.

When addition of La into TNXCNS-0La alloy is increased to 0.12 wt.%, element distribution of Ni, Sn, and La in TNXCNS-0.12La alloy is similar to that in TNXCNS-0.06La alloy, shown in Fig. 3c. However, elements Ni and Sn in α-Cu is 14.80 and 8.50 %, re-

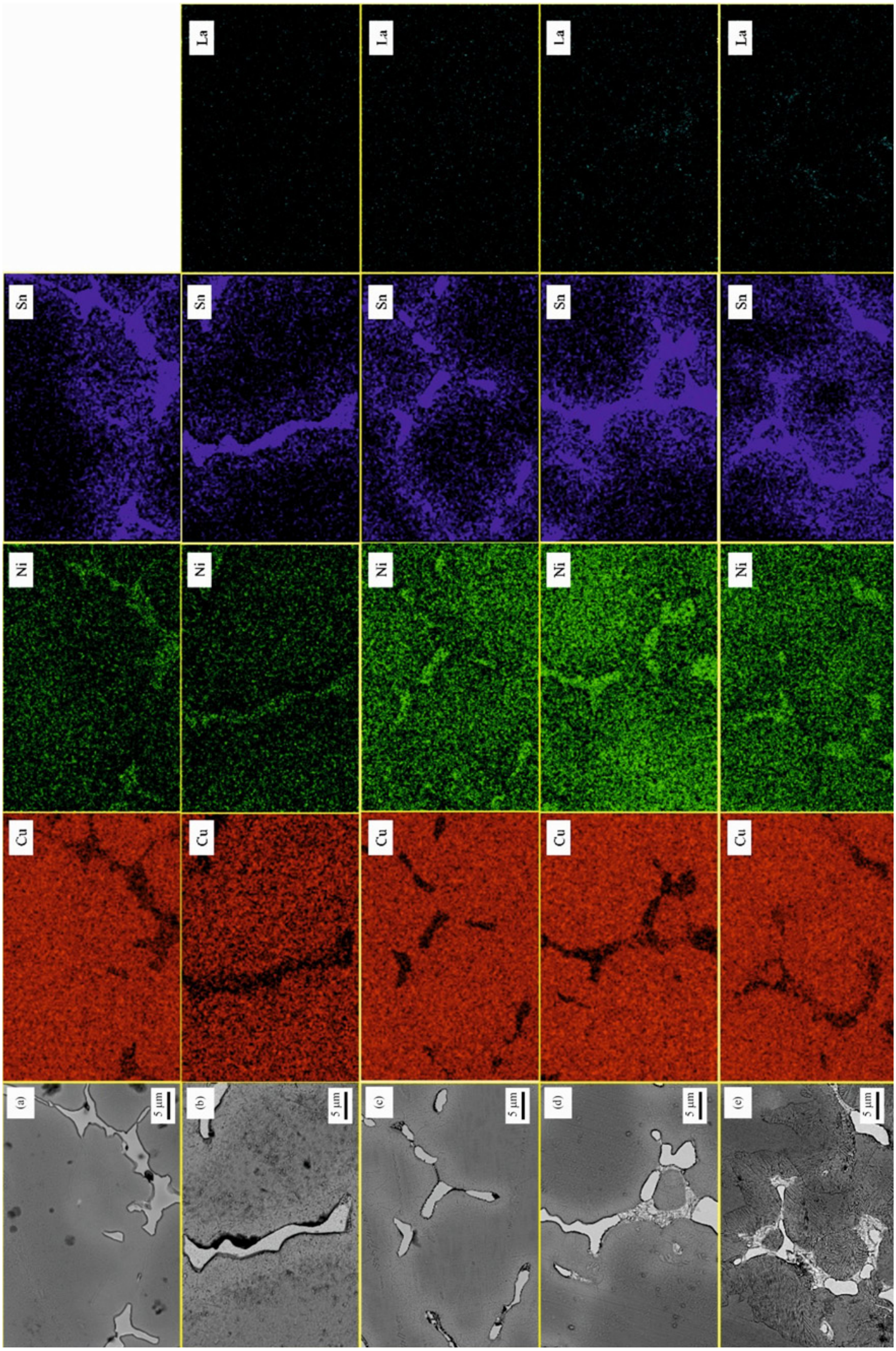

Fig. 3. EDS surface scan spectra of TNXCNS-xLa alloys: (a) TNXCNS-0La, (b) TNXCNS-0.06La,(c) TNXCNS-0.12La,(d) TNXCNS-0.18La, and (e) TNXCNS-0.24La.

spectively, and element Ni in $(\alpha + \gamma)$ eutectic area is 18.27 at.%, while that of element Sn is 15.01 at.%. And element Ni in γ-(Ni,Cu)$_3$Sn phase is slightly changed to 30.73 at.%, while that of element Sn is 25.89 at.%. Additionally, content of La in $(\alpha + \gamma)$ eutectic area and γ-(Ni,Cu)$_3$Sn phase is increased to 0.11 and 0.19 at.%, respectively. Therefore, difference in content of elements Ni and Sn in different phases are further smaller, and elemental segregation of TNXCNS-0La alloy is consequently reduced.

When addition of La into TNXCNS-0La alloy is increased to 0.18 and 0.24 wt.%, element distribution in TNXCNS-0.18La alloy and TNXCNS-0.24La alloy is quite similar to each other. Element Ni in the alloys is also mainly rich in γ-(Ni,Cu)$_3$Sn phase, and element Sn is also mainly distributed in γ-(Ni,Cu)$_3$Sn phase and $(\alpha + \gamma)$ eutectic area, and element La is slightly segregated in γ-(Ni,Cu)$_3$Sn phase of the alloys, shown in Figs. 3d,e. However, element Ni in α-Cu of TNXCNS-0.18La alloy and TNXCNS-0.24La alloy is 13.02 and 13.73 %, respectively, and element Sn in α-Cu of the alloys is 6.75 and 5.41 %, respectively. Element Ni in $(\alpha+\gamma)$ eutectic area of the alloys is 18.28 and 18.43 at.%, while that of element Sn is 12.37 and 9.91 at.%. Elements Ni and Sn in γ-(Ni,Cu)$_3$Sn phase of the alloys are no obvious change. And content of La in $(\alpha + \gamma)$ eutectic area of the alloys is increased to 0.14 and 0.20 at.%, while that in γ-(Ni,Cu)$_3$Sn phase is increased to 0.25 and 0.29 at.%, respectively.

Therefore, addition of La can first reduce then increase element segregation of Ni and Sn in TNXCNS-xLa alloys. The above phenomenon is mainly attributed to grain refinement and microstructure evolution caused by addition of La. As reported by Lu [29], addition of rare earth Y can lead to transformation of $(\alpha + \gamma)$ eutectic area from lamellar to granular shape, and refine grain size by formation of intermetallics containing rare earth Y, therefore reduce segregation of Sn in the Cu-12.5Ni-5Sn alloys. Similarly, when addition of La is less than 0.12 wt.%, addition of La can lead to certain transformation of $(\alpha+\gamma)$ eutectic area from lamellar to granular shape and structure refinement with average dendrite spacing from 51.1 to 32.3 μm caused by formation of LaNiSn phase. Therefore, segregation of Ni and Sn in the alloys is reduced. However, when addition of La is higher than 0.12 wt.%, dimensional size of LaNiSn phase formed in the alloys is getting bigger, which can conversely increase segregation of Ni and Sn in the alloys.

3.4. *Mechanical properties of TNXCNS-xLa alloys*

Microhardness tests and room-temperature tensile tests were conducted on alloys with varying La contents, shown in Fig. 4. Results show that microhardness TNXCNS-xLa alloys first increases then decreases with increasing La content, shown in Fig. 4a. Microhardness of TNXCNS-0La alloy without addition of La is 121 HV. Microhardness of the TNXCNS-0.06La alloy with addition of 0.06wt.%La is increased to 167.6 HV, representing a significant increase of 38.5 % compared to that of the alloy without La added. When addition of La increased to 0.12 wt.%La, microhardness of TNXCNS-0.12La alloy reaches maximum of 192.8 HV, which is improved by 59.3 % compared with that of the alloy without La added. When content of La is increased to 0.18 wt.%, microhardness of TNXCNS-0.18La alloy decreases to 183.2 HV, which is an increase of 51.4 % compared with the La-free alloy. By increasing content of rare earth to 0.24 wt.%La, microhardness of TNXCNS-0.24La alloy further decreases to 175.8 HV, which is 45.2 % higher than that of the La-free alloy. Therefore, addition of rare earth La can increase microhardness TNXCNS-xLa alloys.

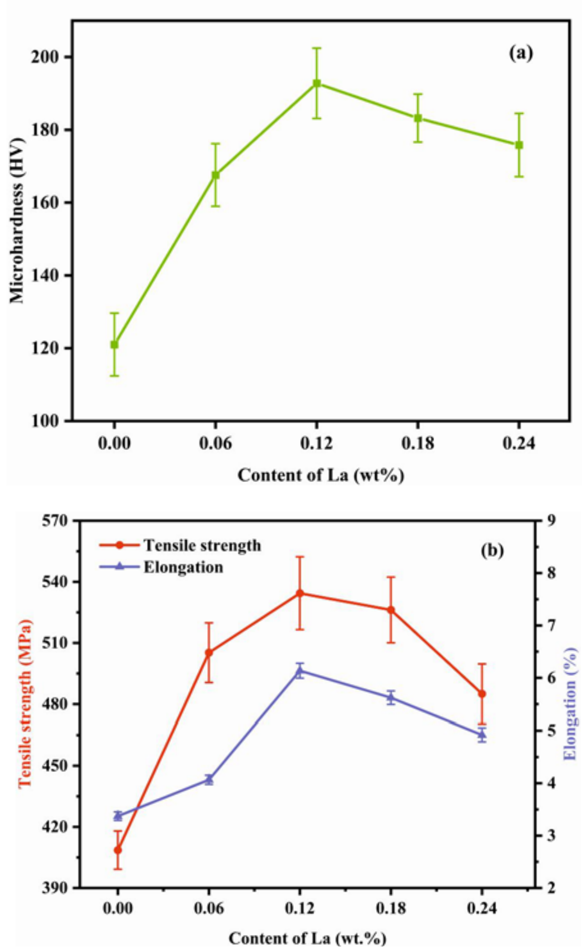

Fig. 4. Mechanical properties of TNXCNS-xLa alloys with different La content: (a) microhardness and (b) tensile strength and elongation.

Both the tensile strength and elongation of the TNXCNS-xLa alloys exhibits an initial increasing trend followed by a subsequent decreasing tendency with increasing of La content added to the TNXCNS-0La alloy, shown in Fig. 4b. Tensile strength of TNXCNS-0La alloy without addition of La is 408.6 MPa and elongation of the alloy is 3.37 %. Tensile strength of TNXCNS-0.06La alloy with addition of 0.06wt.%La is increased to 505.2 MPa and the elongation is increased to 4.07 %, which are increased by 23.6 and 20.8 % compared to that of the alloy without rare earth La addition. When La addition into TNXCNS-0La alloy is increased to 0.12 wt.%, tensile strength of TNXCNS-0.12La alloy reaches the highest of 534.4 MPa and elongation of the alloy after fracture reaches the maximum of 6.14 %, which are increased by 30.8 and 82.2 % compared to that of the alloy without rare earth La addition.

When La addition into TNXCNS-0La alloy is increased to 0.18 wt.%, tensile strength of TNXCNS-0.18La alloy decreases slightly to 526.2 MPa and elongation of the alloy decreases to 5.62 %, which are increased by 28.8 and 66.8 % compared with that of the alloy without rare earth La addition. When La addition into TNXCNS-0La alloy is further increased to 0.24 wt.%, tensile strength of TNXCNS-0.24La alloy further decreases to 485 MPa, and the elongation of the alloy is decreased to 4.92 %, which are increased by 18.7 and 46 % compared with that of the alloy without rare earth La addition. Therefore, TNXCNS-0.12La alloy with addition of 0.12wt.%La exhibits the best comprehensive mechanical properties among the TNXCNS-xLa alloys.

Mechanical properties of TNXCNS-0La alloys are affected by different mechanism for addition of rare earth La. When addition of La into TNXCNS-0La alloy is 0.06 wt.%, no secondary phase form in TNXCNS-0.06La alloy, however, the TNXCNS-0.06La alloy is obviously refined by addition of 0.06wt.%La, therefore, the mechanical properties is improved by grain refining effect and solid solution strengthening effect. When addition of La into TNXCNS-0La alloy increases to 0.12 wt.%, rare earth La can react with element Ni and Sn to form LaNiSn phase, which can act as heterogeneous nucleus of TNXCNS-0.12La alloy and refine grains of the alloy by decreasing average dendrite spacing from 51.1 to 32.3 µm.

The above results is consistent with previous research that mechanical properties of Cu-12.5Ni-5Sn alloy can be improved by grain refining effect caused by formation of secondary phase for addition of rare earth Y [30]. Furthermore, addition of 0.12wt.%La into TNXCNS-0La alloy can effectively reduce elemental segregation of Sn and Ni, therefore is benefit for improvement of mechanical properties.

When addition of La into TNXCNS-0La alloy exceed 0.12 wt.%, hardness, tensile strength and elongation of the alloys decrease. The above result can be attributed to growth of LaNiSn phase caused by excessive addition of La, which is consistent with the research that excessive addition of Ti into TNXCNS-0La alloy will form coarse Ni_3Ti phase and decrease its mechanical properties. The coarse LaNiSn phase will decrease the grain refinement effect and decrease its mechanical properties. However, tensile strength of TNXCNS-0.24La alloy is still higher than that of TNXCNS-0La alloy for positive effect of rare earth La addition.

4. Conclusions

(1) New LaNiSn phase is formed in alloys with La content of 0.12 wt.%, and the dimensional size of the new LaNiSn phase increases with increasing of La content. Dendrite spacing of the alloys is first decreased and then increased by addition of La, dendrite spacing of alloy with addition of 0.12wt.%La is the smallest of 32.3 µm.

(2) Element segregation of different areas first decrease then increase with increase of La added into the Cu-15Ni-8Sn-xLa alloys, and the TNXCNS-0.12La alloy with addition of 0.12wt.%La is the smallest for the grain refinement effect and transformation of $(\alpha + \gamma)$ regions from lamellar to granular shape.

(3) Hardness, tensile strength, and ductility of the alloys exhibits an initial increasing trend followed by a subsequent decreasing tendency with the gradual increase of La content. The alloy with 0.12wt.%La addition exhibits the optimal comprehensive mechanical properties, with the hardness, tensile strength and ductility reaching 192.8 HV, 534.4 MPa, and 6.14 %, respectively.

Acknowledgements

This work was supported by National Natural Science Foundation of China (Grant No. 52425401), Program for Science & Technology Innovation Talents in Universities of Henan Province (NO. 23HASTIT022) and The fund of Henan Key Laboratory of Superhard Abrasives and Grinding Equipment, Henan University of Technology (NO. JDKFJJ2024003).

References

[1] R. Ravichandran, N. Rajendran, Electrochemical behaviour of brass in artificial seawater: effect of organic inhibitors, Applied Surface Science 241 (2005) 449–458. https://doi.org/10.1016/j.apsusc.2004.07.046

[2] J. Caris, R. Varadarajan, J. J. Stephens Jr, J. J. Levandowski, Microstructural effects on tension and fatigue behavior of Cu-15Ni-8Sn sheet, Materials Science and Engineering: A 491 (2008)137–146. https://doi.org/10.1016/j.msea.2008.01.061

[3] J. B. Singh, W. Cai, P. Bellon, Dry sliding of Cu-15wt%Ni-8wt% Sn bronze: Wear behaviour and microstructures, Wear 263 (2007) 830–841. https://doi.org/10.1016/j.wear.2007.01.061

[4] J. Miettinen, Thermodynamic description of the Cu-Ni-Sn system at the Cu-Ni side, Calphad 27 (2003) 309–318. https://doi.org/10.1016/j.calphad.2003.10.001

[5] Y. Liao, M. Xie, H. Chen, W. Xie, H. Wang, B. Yang, Thermodynamics and kinetics of discontinuous precipitation in Cu-9Ni-xSn alloy, Journal of Alloys and Compounds 827 (2020) 154314. https://doi.org/10.1016/j.jallcom.2020.154314

[6] J. Hang, Z. Guo, J. Jie, J. Cheng, D. Zhang, Evolution behavior of γ-$D0_3$ phase in Cu-15Ni-8Sn alloy and the corresponding effects on alloy property, Journal of Alloys and Compounds 897 (2022) 162736. https://doi.org/10.1016/j.jallcom.2021.162736

[7] C. Guo, J. Wan, J. Chen, X. Xiao, H. Huang, J. Liu, B. Yang, Inhibition of discontinuous precipitation and enhanced properties of Cu–15Ni–8Sn alloy with Fe addition, Materials Science and Engineering: A 795 (2022) 139917. https://doi.org/10.1016/j.msea.2020.139917

[8] C. Guo, Y. Shi, J. Chen, X. Xiao, B. Liu, J. Liu, B. Yang, Effects of P addition on spinodal decomposition and discontinuous precipitation in Cu-15Ni-8Sn alloy, Materials Characterization 171 (2021) 110760. https://doi.org/10.1016/j.matchar.2020.110760

[9] J. Cheng, M. Mao, X. Gan, Q. Lei, Z. Li, K. Zhou, Microstructures, mechanical properties, and grease-lubricated sliding wear behavior of Cu-15Ni-8Sn-0.8Nb alloy with high strength and toughness, Friction 9 (2020) 1061–1076. https://doi.org/10.1007/s40544-020-0399-7

[10] Y. Ouyang, X.-P. Gan, S.-Z. Zhang, Z. Li, K.-C. Zhou, Y.-X. Jiang, X.-W. Zhang, Age-hardening behavior and microstructure of Cu-15Ni-8Sn-0.3Nb alloy prepared by powder metallurgy and hot extrusion, Transactions of Nonferrous Metals Society of China 27 (2017) 1947–1955. https://doi.org/10.1016/S1003-6326(17)60219-X

[11] C. Zhao, W. Zhang, Z. Wang, D. Li, Z. Luo, C. Yang, D. Zhang, Improving the mechanical properties of Cu-15Ni-8Sn alloys by addition of titanium, Materials 10 (2017) 1038. https://doi.org/10.3390/ma10091038

[12] Z. Guo, J. Jie, S. Liu, Y. Zhang, B. Qin, T. Wang, T. Li, Effect of V addition on microstructures and mechanical properties of Cu-15Ni-8Sn alloy, Materials Science and Engineering: A 748 (2019) 85–94. https://doi.org/10.1016/j.msea.2019.01.084

[13] W. Luo, L.-J. Peng, X.-J. Mi, H.-F. Xie, Y.-C. Cao, S.-H. Huang, Precipitation evolution and properties of Cu-15Ni-8Sn alloys via Al microalloying during ageing, Rare Metals 43 (2024) 5216–5228. https://doi.org/10.1007/s12598-024-02761-2

[14] K. Zhang, L. Zhang, C. Shu, W. Fan, S. Li, X. Juan, J. Zhao, Y. Wang, Effect of different Mo addition on microstructure and mechanical properties of Cu-15Ni-8Sn alloy, Materials 15 (2022) 5521. https://doi.org/10.3390/ma15165521

[15] N. J. Li, X. N. Li, Z. M. Li, Q. X. Yu, Y. H. Zheng, Y. L. Hu, Q. Wang, C. Dong, Y. X. Jiang, X. W. Zhang, Differential effects of Zn and Co solutes on the properties of Cu-Ni-Sn alloys, Intermetallics 125 (2020) 106894. https://doi.org/10.1016/j.intermet.2020.106894

[16] S. Liu, Z. Guo, S. Zhang, J. Jie, S. Xu, X. Li, T. Li, Effect of B addition on microstructures and properties of Cu-15Ni-8Sn alloy, Journal of Alloys and Compounds 947 (2023) 169644. https://doi.org/10.1016/j.jallcom.2023.169644

[17] Q. X. Yu, X. N. Li, K. R. Wei, Z. M. Li, Y. H. Zheng, N. J. Li, X. T. Cheng, C. Y. Wang, Q. Wang, C. Dong, Cu-Ni-Sn-Si alloys designed by cluster-plus-glue-atom model, Materials & Design 167 (2019) 107641. https://doi.org/10.1016/j.matdes.2019.107641

[18] R. Tholkappiyan, K.Vishista, Influence of lanthanum on the optomagnetic properties of zinc ferrite prepared by combustion method, Physica B: Condensed Matter 448 (2014) 177–183. https://doi.org/10.1016/j.physb.2014.04.022

[19] F. Hamed, T. Ramachandran, V. Kurapati, The effect of induced strains on the optical band gaps in lanthanum-doped zinc ferrite nanocrystalline powders, Modern Physics Letters B 30 (2016) 1650230. https://doi.org/10.1142/S0217984916502304

[20] F. A. Guo, C. J. Xiang, C. X. Yang, X. M. Cao, S. G. Mu, Y. Q. Tang, Study of rare earth elements on the physical and mechanical properties of a Cu-Fe-P-Cr alloy, Materials Science and Engineering: B 147 (2008) 1–6. https://doi.org/10.1016/j.mseb.2007.10.011

[21] X. Mao, F. Fang, J. Jiang, R. Tan, Effect of rare earth on the microstructure and mechanical properties of as-cast Cu-30Ni alloy, Rare Metals 28 (2009) 590–595. https://doi.org/10.1007/s12598-009-0113-4#citeas

[22] Y. Chen, M. Cheng, H. Song, S. Zhang, J. Liu, Y. Zhu, Effects of lanthanum addition on microstructure and mechanical properties of as-cast pure copper, Journal of Rare Earths 32 (2014) 1056–1063. https://doi.org/10.1016/S1002-0721(14)60183-6

[23] J. Li, L. Chang, S. Li, X. Zhu, Z. An, Microstructure and properties of as-cast Cu-Cr-Zr alloys with lanthanum addition, Journal of Rare Earths 36 (2018) 424–429. https://doi.org/10.1016/j.jre.2017.11.006

[24] P. H. Hu, H. W. Song, S. W. Wang, Y. Chen, S. H. Zhang, Mechanisms of primary phase refinement and toughness improvement of Cu-2wt%Ag-0.15wt%La alloy through continuous extrusion forming, Materials Science and Engineering: A 819 (2021) 141521. https://doi.org/10.1016/j.msea.2021.141521

[25] N. Wang, Y. Shen, Q. An, K. Mahdav Reddy, M. Jin, R. Karre, X. Wang, Microstructure evolution and mechanical property of Cu-15Ni-8Sn-0.2Nb alloy during aging treatment, Journal of Materials Science & Technology 86 (2021) 227–236. https://doi.org/10.1016/j.jmst.2021.01.034

[26] A. Takeuchi, A. Inoue, Classification of bulk metallic glasses by atomic size difference, heat of mixing and period of constituent elements and its application to characterization of the main alloying element, Materials Transactions 46 (2005) 2817–2829. https://doi.org/10.2320/matertrans.46.2817

[27] L. Shao, T. Zhang, L. Li, Y. Zhao, J. Huang, P. K. Liaw, Y. Zhang, A low-cost lightweight entropic alloy with high strength, Journal of Materials

Engineering and Performance 27 (2018) 6648–6656. https://doi.org/10.1007/s11665-018-3720-0
[28] X. K. Chen, X. P. Xiao, D. W. Yuan, J. Chen, Y. Wu, Effect of Ni/Sn ratio on microstructure and properties of Cu-Ni-Sn-P alloy, Scientific Reports 14 (2024) 31609. https://doi.org/10.21203/rs.3.rs-4144242/v1
[29] S. Lu, S. Du, X. Wang, Z. Ding, X. Liu, Z. Li, Microstructure and mechanical properties of Cu-Ni-Sn alloy regulated by trace rare earth element Y, Materials Characterization 217 (2024) 114334. https://doi.org/10.1016/j.matchar.2024.114334
[30] X. Liu, Z. Li, G. Yang, Q. Wang, S. Lu, G. Yang, J. Wang, Effect of rare earth element Y addition on the corrosion resistance of Cu-12.5Ni-5Sn alloy after aging, Journal of Alloys and Compounds 1004 (2024) 175905. https://doi.org/10.1016/j.jallcom.2024.175905